# A Multiscale, Multiphysics Approach to Vertical-cavity Surface-emitting Laser Simulation

**A. Tibaldi**[1], **F. Bertazzi**[1,2], **M. Goano**[1,2],
**M. Daubenschüz**[3], **R. Michalzik**[4], **and P. Debernardi**[2]

[1]Dipartimento di Elettronica e Telecomunicazioni, Politecnico di Torino
Corso Duca degli Abruzzi 24, Torino 10129, Italy
[2]Istituto di Elettronica e di Ingegneria dell'Informazione e delle Telecomunicazioni (IEIIT)
Consiglio, Nazionale delle Ricerche (CNR), Corso Duca degli Abruzzi 24, Torino 10129, Italy
[3]Philips Photonics GmbH, Lise-Meitner-Straße 13, Ulm 89081, Germany
[4]Institute of Functional Nanosystems, Ulm University
Albert-Einstein-Allee 45, Ulm 89081, Germany

**Abstract**— The lasing operation of vertical-cavity surface-emitting lasers (VCSELs) results from the interaction of diverse physical mechanisms. For this reason, a reliable model must solve the coupled carrier transport, thermal and optical problems. With the aim of removing the present lack of established simulation tools, in this work we present our in-house electro-opto-thermal VCSEL numerical simulator VENUS. After a description of its four constituents, a validation with experimental results obtained at different temperatures is presented, demonstrating the predictive capabilities of VENUS.

## 1. INTRODUCTION

Mainly driven by the pervasiveness of smartphones in our daily lives, the last few years have witnessed an increasingly growing number of applications for low-power microlasers. This is why at present there are over 2 billion vertical-cavity surface-emitting lasers (VCSELs) in use, and many hundred millions produced every year to face their ever increasing demand [1–4]. Further expanding the VCSELs' horizon will require exploring new material systems and, at the same time, novel geometries. For this reason, the availability of computer-aided design modeling tools is going to be a strategic asset in the next future, as a support or replacement of experimental prototyping.

Figure 1(a) shows a typical oxide-confined AlGaAs VCSEL geometry. Optically, this structure is a resonator, whose mirrors are distributed Bragg reflectors (DBRs) alternating quasi-GaAs to quasi-AlAs $\lambda/4$ layers. On the other hand, from the electrical standpoint, this geometry is basically a complex *pin* diode: the top and bottom mirrors are, respectively, *p*- and *n*-doped, current is injected at the annular *p*-contact and flows through the top DBR, then it gets focused by the oxide aperture and feeds the quantum wells; finally, it goes through the *n*-doped part to the bottom contact. Finally, the presence of current and of recombination and optical absorption processes causes the device self-heating, which affects all the quantities in play (refractive index, mobility and so on).

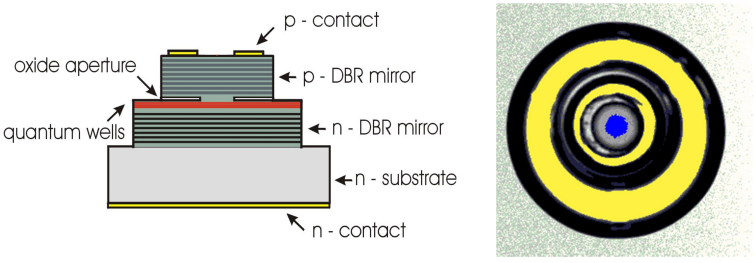


Figure 1: (a) sketch of an oxide-confined AlGaAs VCSEL, indicating all its relevant geometry details. (b) top view of the device under investigation, where the contact ring (12 µm diameter) and the oxide aperture (4 µm diameter) are colored in yellow and blue, respectively.

From this description, it should be clear that the VCSEL operation involves the entangled interplay of optics, electronics and thermal conduction, so that developing a comprehensive VCSEL model is a rather challenging task. Even if the literature reports several valuable optical or electrical simulators, almost no truly self-consistent multiphysics tool is currently available, also including commercial simulation codes. Standing on the shoulders of the seminal work by Hadley et al. [5], research groups worldwide developed many multiphysics VCSEL models [6–10]. The common denominator of these works is the phenomenological treatment of carrier injection, which is described by rate equations. A more rigorous treatment of carrier transport in VCSELs was proposed by Streiff et al. [11] and recently by Mehta et al. [12]. Among the commercially available softwares, previous versions of ISE TCAD [13] featured the model described by Streiff, but at present it is no longer supported nor documented [14]. Sentaurus could be potentially coupled to LaserMOD [15] from Synopsys RSoft, whose optical solver is scalar. Another commercial modeling suite that can be used for VCSEL simulation is PICS3D [16] from Crosslight Software.

In an effort to advance in this field and eliminate the lack of reliable VCSEL CAD tools, this paper presents our VCSEL Electro-opto-thermal Numerical Simulator VENUS [17]. After reviewing the four VENUS constituents, a validation with experimental results is presented and discussed.

## 2. VENUS CONSTITUTIVE BLOCKS

VENUS consists of four fundamental blocks: an optical mode solver, a description of the spontaneous and stimulated emission in the active region, a thermal simulator, and a carrier transport model, which will be briefly described in the following. Additional details on VENUS can be found in [17].

### 2.1. VELM: Optical Mode Solver

The optical solver is the 3D vectorial Vcsel ELectroMagnetic (VELM) simulator [18, 19]. It is based on representing the electromagnetic field as a superposition of the TE and TM modes of a reference medium in cylindrical coordinates. The transverse details of the structures are described as variations to such reference medium and are accounted for by coupled-mode theory, allowing to describe each layer constituting the VCSEL stack by means of a transmission matrix. By cascading such transmission matrices one can compute the overall transmission matrix between the two radiating sections, beyond which the device can be considered homogeneous. The electromagnetic problem is closed by introducing appropriate boundary conditions relating backward to forward waves at the ending sections. An eigenvalue problem can be obtained by enforcing the self-consistency condition of the field subject to a full-cavity round-trip, whose complex eigenvalues represent the modal wavelengths and the corresponding threshold gains (real and imaginary parts, respectively), and whose eigenvectors are the expansion coefficients of the electromagnetic field in the cylindrical wave basis. VELM has been validated through a comparison with other simulation tools [20], and with experiments [21–28].

### 2.2. Quantum Well Optical Response: Gain and Spontaneous Emission

Describing the optical processes occurring in the quantum well (QW) active region of a VCSEL requires the evaluation *a priori* of the nanostructure subbands. A good trade-off between oversimplifications such as the effective mass approximation and computationally-expensive frameworks like the density functional theory is given by solving the Schrödinger equation with a $\mathbf{k} \cdot \mathbf{p}$ Hamiltonian and a potential defined by the nanostructure composition and geometry. The subbands and the envelope functions are then found as the solutions of the resulting eigenvalue problem. More specifically, our work is derived from the Burt-Foreman finite element formulation used to get rid of spurious subbands [29, 30]. Then, by assuming axial symmetry and block-diagonalizing the so-approximated Hamiltonian, a 4-band approach is obtained (heavy holes, light holes, split-off and electrons), where spin degeneracy is accounted for *a posteriori* [31, 32].

Stimulated and spontaneous emission spectra as well as the refractive index change induced by carrier injection are evaluated through Fermi's golden rule, including also a many-body description of the carrier-induced bandgap shrinkage within the Hartree-Fock approximation [33]. Here, scattering relaxation is described phenomenologically as a lineshape broadening. In this context, several approaches have been investigated, including the widely-used Lorentzian [34, 35] and Landsberg models [36, 37]. In this work we follow the approach by Tomita et al. [38], featuring non-Markovian effects, since it provides the best agreement with the experimental laser operation curves.

### 2.3. Thermal Solver

By studying the typical temperature profile in a VCSEL, it is possible to identify two regions characterized by very different behaviors: the substrate, where temperature decays almost linearly toward the heat sink, and the active part of the device, where strong temperature gradients can be observed. A numerical scheme exploiting this observation is the spectral element method (SEM) [39]. As in the standard finite element method (FEM), a linear system is achieved by expanding the unknown temperature and projecting the heat equation as a superposition of known basis functions. The peculiarity of the SEM is to use a low $h$-refinement, i.e., dividing the domain in few subdomains, making instead use of a strong $p$-refinement, which means using high-order basis functions. This strategy is particularly effective for the VCSEL heat equation, as it can be applied with different numerical resolutions in different subdomains, allowing to optimize the basis within each interval and leading to fast and accurate simulations.

### 2.4. Quantum-corrected Drift-diffusion

In several comprehensive VCSEL simulators, carrier injection in the active region is modeled by means of phenomenological rate equations, treating the VCSEL as a generic dynamical system [5–10, 40]. A rigorous description should picture how carriers, after flowing through bulky semiconductor regions such as the distributed Bragg reflectors (DBRs), scatter into the quantum well confined states and then participate in radiative processes. A rigorous treatment of these phenomena would then require at least high-order quantum-corrected semiclassical techniques [41–43], or more appropriately genuine quantum-kinetic frameworks based on density matrix (DM) or on nonequilibrium Green's function (NEGF) approaches [33], which is utopian for an entire VCSEL. A sensible trade-off between these models is given by drift-diffusion, which is quite consolidated in both academic and industry contexts for simulating electronic devices. A system of nonlinear equations is achieved by the Scharfetter-Gummel finite-box discretization, and it is then solved by a generalized Newton's method [44, 45].

In view of applying drift-diffusion to lasers, the model must be augmented with photon rate equations describing the interplay of carrier transport and the optical models. This is coupled to the continuity equations through a stimulated recombination rate, which is added to the usual Shockley-Read-Hall, radiative and Auger terms. In addition to the classical treatment of heterostructures [46], an improved description of the active region has been implemented by introducing quantum corrections accounting for the bulk-bound carrier dynamics [33, 47, 48]. These approaches have been investigated by several groups [11, 49–54], but it is still a hot research subject [55–58]. Bound carriers are distributed along the quantum-confined direction according to their envelope eigenfunctions, while in the lateral direction it is reasonable to describe their transport by standard drift-diffusion. However, the determination of the model parameters, namely the electron and hole mobilities and their thermal dependence is critical [59], as they play a crucial role in the spatial hole burning mode competition [60].

It is to be remarked that only the electrical solver relies on an extensive spatial discretization, while both thermal and optical solvers are based on modal expansions. For this reason no grid adaptation steps are required at all, reducing the multiphysics couplings to the simple evaluation of the optical and thermal expanded quantities at the drift-diffusion mesh points. Still, simulating the entire VCSEL, including each DBR layer, requires around 60,000 mesh points, corresponding to linearized systems three times larger (including the discretized Poisson, electron, and hole continuity equations). Although such simulations are still feasible, the computational burden can be lightened by replacing most of the DBR layers with an average material, reducing the problem dimension at least by a factor 2 [61].

## 3. NUMERICAL AND EXPERIMENTAL RESULTS

This section presents an experimental validation of VENUS performed on an oxide-confined AlGaAs VCSEL manufactured at Philips Photonics. The VCSEL is grown on an $n$-doped GaAs substrate later thinned to 110 µm. The device includes a $1\lambda$-cavity with three 8 nm GaAs quantum wells, placed at the maximum of the optical standing wave. The 30 nm oxide layer is placed in the first of the 21 pairs of the $p$-DBR outcoupling mirror; the bottom $n$-doped DBR includes 37 pairs. Composition and doping gradings are introduced in both mirrors to enhance electrical conduction and minimize free-carrier absorption. A 26 µm diameter mesa is etched to realize the 4 µm oxide aperture by the oxidation of the quasi-AlAs layer; later, a passivation layer is deposited to insulate the mesa sides and reduce the parasitic capacitance. Current is injected through the

12 µm diameter metal ring top contact. Figure 1(b) shows a camera image of the top side of the device under investigation, where the contact ring and the oxide aperture are colored in yellow and blue, respectively.

Since VCSELs can be found in the most disparate applications, from smartphones to data center racks, it is fundamental to demonstrate the VENUS capability to predict lasing operation over broad temperature ranges. This has been carried out by connecting the VCSEL bottom contact to a Peltier element, which allows to set the heat sink temperature. In this view, Figure 2 reports the (a) *IV* and (b) *LI* characteristics, and (c) the differential resistance and (d) wavelength versus current. The cyan, blue, green, and red curves are obtained for 20°C, 50°C, 80°C, and 110°C Peltier cell temperatures; the numerical and experimental results are distinguished with solid and dotted curves.

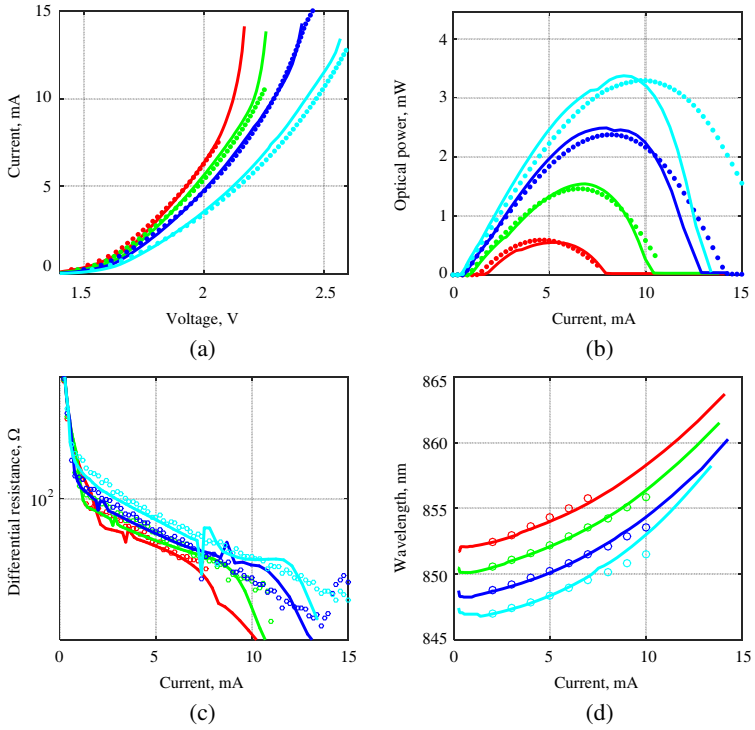


Figure 2: Results of the numerical (solid curves) and experimental (dots) investigations performed on the VCSEL described in the text. (a) *IV* chracteristics; (b) *LI* characteristics; (c) differential resistance versus current; (d) wavelength red-shift versus current. The different results refer to different Peltier cell temperatures: the cyan, blue, green, and red curves are obtained for 20°C, 50°C, 80°C, and 110°C, respectively.

The results presented in Figure 2 have been obtained after a careful calibration of the model parameters. A good agreement between numerical and experimental results has been achieved. The simulated *IV* characteristics, which are strongly related to carrier mobilities and recombination rates, fit well the experimental results until the device turns off. The effect of Auger recombinations was deeply investigated [62–65], since it has rather different impacts at the different temperatures [66]. This is fundamental to achieve a reasonable agreement also for the resistance characteristics, which report the same information as the *IV* curve, but are much more sensitive to the model parameters due to their differential nature. The wavelength red-shift is the *thermometer* of the device, as it provides the only observable directly connected to heating. In addition to the thermal dependence of each optical and electrical model, which influences the heat sources, particular care must be dedicated to a correct choice of the thermal conductivities, which differ from their nominal values due to phonon reflection phenomena occurring in the DBR superlattices [67, 68]. Moreover, it is fundamental to take into account also the temperature dependence of thermal conductivity [69]. The *LI* characteristics exhibit a strong dependence on all the aforementioned model parameters. This is evident for instance when looking at the 20°C curve, which agrees very well until the rollover, from which the optical power drop is overestimated, as a consequence of the predicted overheating.

## 4. CONCLUSIONS

This work describes the VCSEL electro-opto-thermal numerical simulator VENUS. Obtained by coupling state-of-the-art solvers for each of the three physical frameworks, VENUS proved its capability to simulate a real device in less than one hour on a standard personal computer. Comparisons with measurements performed at different heat sink temperatures demonstrated the possibility to predict the *LIV* characteristics over the whole operation range. VENUS is now ready to be applied to the design-oriented analysis of devices with innovative geometries and materials.

## REFERENCES


1. Michalzik, R., ed., *VCSELs: Fundamentals, Technology and Applications of Vertical-Cavity Surface-Emitting Lasers*, Springer-Verlag, Berlin, 2013.
2. Moench, H., M. Carpaij, P. Gerlach, S. Gronenborn, R. Gudde, J. Hellmig, J. Kolb, and A. van der Lee, "VCSEL based sensors for distance and velocity," *Proc. SPIE*, Vol. 9766, 97 660A–1–16, 2016.
3. Ebeling, K. J., R. Michalzik, and H. Moench, "Vertical-cavity surface-emitting laser technology applications with focus on sensors and three-dimensional imaging," *Japan. J. Appl. Phys.*, Vol. 52, 08PA02–1–11, 2018.
4. Chow, W. W. and S. Reitzenstein, "Quantum-optical influences in optoelectronics — An introduction," *Appl. Phys. Rev.*, Vol. 5, 041 302–1–22, 2018.
5. Hadley, G. R., K. L. Lear, M. E. Warren, K. D. Choquette, J. W. Scott, and S. W. Corzine, "Comprehensive numerical modeling of vertical-cavity surface-emitting lasers," *IEEE J. Quantum Electron.*, Vol. 32, No. 4, 607–616, 1996.
6. Conradi, O., S. Helfert, and R. Pregla, "Comprehensive modeling of vertical-cavity laser diodes by the method of lines," *IEEE J. Quantum Electron.*, Vol. 37, No. 7, 928–935, 2001.
7. Gustavsson, J. S., J. A. Vukusic, J. Bengtsson, and A. Larsson, "A comprehensive model for the modal dynamics of vertical-cavity surface-emitting lasers," *IEEE J. Quantum Electron.*, Vol. 38, No. 2, 203–212, 2002.
8. Nyakas, P., G. Varga, Z. Puskás, N. Hashizume, T. Kárpáti, T. Veszprémi, and G. Zsombok, "Self-consistent real three-dimensional simulation of vertical-cavity surface-emitting lasers," *J. Opt. Soc. Amer. B*, Vol. 23, No. 9, 1761–1769, 2006.
9. Debernardi, P., "HOT-VELM: A comprehensive and efficient code for fully vectorial and 3-D hot-cavity VCSEL simulation," *IEEE J. Quantum Electron.*, Vol. 45, No. 8, 979–992, 2009.
10. Sarzala, R., T. Czyszanowski, M. Wasiak, M. Dems, L. Piskorski, W. Nakwaski, and K. Panajotov, "Numerical self-consistent analysis of VCSELs," *Advances in Optical Technologies*, Vol. 2012, 689 519–1–17, 2012.
11. Streiff, M., A. Witzig, M. Pfeiffer, P. Royo, and W. Fichtner, "A comprehensive VCSEL device simulator," *IEEE J. Select. Topics Quantum Electron.*, Vol. 9, No. 3, 879–891, 2003.
12. Mehta, K., Y.-S. Liu, J. Wang, H. Jeong, T. Detchprohm, Y. J. Park, S. R. Alugubelli, S. Wang, F. A. Ponce, S.-C. Shen, R. D. Dupuis, and P. D. Yoder, "Lateral current spreading in III-N ultraviolet vertical-cavity surface-emitting lasers using modulation-doped short period superlattices," *IEEE J. Quantum Electron.*, Vol. 54, No. 4, Art. 2400507, Aug. 2018.
13. *ISE TCAD Release 10.0*, Integrated Systems Engineering AG, Zurich, Switzerland, 2004.
14. *Sentaurus Device User Guide. Version M-2017.09*, Synopsys, Inc., Mountain View, CA, Sept. 2017.
15. *RSoft LaserMOD User Guide, v2018.03*, Synopsys, Inc., Optical Solutions Group, Ossining, NY, 2018.
16. *Crosslight Device Simulation Software. General Manual*, Crosslight Software Inc., Vancouver, BC, Canada, Sept. 2014.
17. Tibaldi, A., F. Bertazzi, M. Goano, R. Michalzik, and P. Debernardi, "VENUS: A Vertical-cavity surface-emitting laser Electro-opto-thermal NUmerical Simulator," *IEEE J. Select. Topics Quantum Electron.*, Vol. 25, No. 6, Art. 1500212, 2019.
18. Bava, G. P., P. Debernardi, and L. Fratta, "Three-dimensional model for vectorial fields in vertical-cavity surface-emitting lasers," *Phys. Rev. A*, Vol. 63, No. 2, Art. 23816, 2001.
19. Debernardi, P. and G. P. Bava, "Coupled mode theory: A powerful tool for analyzing complex VCSELs and designing advanced devices features," *IEEE J. Select. Topics Quantum Electron.*, Vol. 9, No. 3, 905–917, 2003.

20. Bienstman, P., R. Baets, J. Vukusic, A. Larsson, M. J. Noble, M. Brunner, K. Gulden, P. Debernardi, L. Fratta, G. P. Bava, H. Wenzel, B. Klein, O. Conradi, R. Pregla, S. A. Riyopoulos, J.-F. P. Seurin, and S. L. Chuang, "Comparison of optical VCSEL models on the simulation of oxide-confined devices," *IEEE J. Quantum Electron.*, Vol. 37, No. 12, 1618–1631, 2001.
21. Debernardi, P., G. P. Bava, C. Degen, I. Fischer, and W. Elsäßer, "Influence of anisotropies on transverse modes in oxide-confined VCSELs," *IEEE J. Quantum Electron.*, Vol. 38, No. 1, 73–84, 2002.
22. Debernardi, P., G. P. Bava, F. Monti di Sopra, and M. B. Willemsen, "Features of vectorial modes in phase-coupled VCSEL arrays: Experiments and theory," *IEEE J. Quantum Electron.*, Vol. 39, No. 1, 109–119, 2003.
23. Debernardi, P., J. M. Ostermann, M. Sondermann, T. Ackermann, G. P. Bava, and R. Michalzik, "Theoretical-experimental study of the vectorial modal properties of polarization-stable multimode grating VCSELs," *IEEE J. Select. Topics Quantum Electron.*, Vol. 13, No. 5, 1340–1348, 2007.
24. Debernardi, P., R. Orta, T. Gründl, and M.-C. Amann, "3-D vectorial optical model for high-contrast grating vertical-cavity surface-emitting lasers," *IEEE J. Quantum Electron.*, Vol. 49, No. 2, 137–145, 2013.
25. Tibaldi, A., P. Debernardi, and R. Orta, "High-contrast grating performance issues in tunable VCSELs," *IEEE J. Quantum Electron.*, Vol. 51, No. 12, Art. 2400407, 2015.
26. Orta, R., A. Tibaldi, and P. Debernardi, "Bimodal resonance phenomena — Part I: Generalized Fabry-Pérot interferometers," *IEEE J. Quantum Electron.*, Vol. 52, No. 12, 6 100 508–1–8, 2016.
27. Tibaldi, A., P. Debernardi, and R. Orta, "Bimodal resonance phenomena — Part III: High-contrast grating reflectors," *IEEE J. Quantum Electron.*, Vol. 54, No. 6, 6 600 108–1–8, 2018.
28. Debernardi, P., A. Tibaldi, P. Gerlach, P. Martelli, P. Boffi, M. Martinelli, D. Coviello, and R. Orta, "Modal performance of spiral phase plate VCSELs," *IEEE J. Quantum Electron.*, Vol. 52, No. 5, 2 400 108–1–8, 2016.
29. Foreman, B. A., "Elimination of spurious solutions from eight-band $k \cdot p$ theory," *Phys. Rev. B*, Vol. 56, No. 20, R12 748–R12 751, 1997.
30. Zhou, X., F. Bertazzi, M. Goano, G. Ghione, and E. Bellotti, "Deriving $k \cdot p$ parameters from full-Brillouin-zone descriptions: A finite-element envelope function model for quantum-confined wurtzite nanostructures," *J. Appl. Phys.*, Vol. 116, No. 3, Art. 033709, 2014.
31. Liu, G. and S.-L. Chuang, "Modeling of Sb-based type-II quantum cascade lasers," *Phys. Rev. B*, Vol. 65, 165 220–1–10, 2002.
32. Qiao, P.-F., S. Mou, and S.-L. Chuang, "Electronic band structures and optical properties of type-II superlattice photodetectors with interfacial effect," *Opt. Express*, Vol. 20, No. 2, 2319–2334, 2012.
33. Bertazzi, F., M. Goano, G. Ghione, A. Tibaldi, P. Debernardi, and E. Bellotti, "Electron transport," *Handbook of Optoelectronic Device Modeling and Simulation*, J. Piprek, Ed., Chap. 2, 35–80, CRC Press, Boca Raton, FL, 2017.
34. Ahn, D. and S.-L. Chuang, "Optical gain in a strained-layer quantum-well laser," *IEEE J. Quantum Electron.*, Vol. 24, No. 12, 2400–2406, 1988.
35. Chuang, S.-L., *Physics of Photonic Devices*, John Wiley & Sons, Hoboken, 2009.
36. Landsberg, P. T., "Electron interaction effects on recombination spectra," *Phys. Status Solidi B*, Vol. 15, No. 1, 623–626, 1966.
37. Martin, R. W. and H. L. Störmer, "On the low energy tail of the electron-hole drop recombination spectrum," *Solid State Commun.*, Vol. 22, 523–526, 1977.
38. Tomita, A. and A. Suzuki, "A new density matrix theory for semiconductor lasers, including non-Markovian intraband relaxation and its application to nonlinear gain," *IEEE J. Quantum Electron.*, Vol. 27, No. 6, 1630–1641, 1991.
39. Tibaldi, A., R. Orta, O. A. Peverini, G. Addamo, G. Virone, and R. Tascone, "Skew incidence plane-wave scattering from 2-D dielectric periodic structures: Analysis by the mortar-element method," *IEEE Trans. Microwave Theory Tech.*, Vol. 63, No. 1, 11–19, 2015.
40. Debernardi, P., "Three-dimensional modeling of VCSELs," *VCSELs: Fundamentals, Technology and Applications of Vertical-cavity Surface-emitting Lasers*, R. Michalzik, ed., Chap. 3, 77–117, Berlin, Springer-Verlag, 2013.

41. Bertazzi, F., M. Moresco, and E. Bellotti, "Theory of high field carrier transport and impact ionization in wurtzite GaN. Part I: A full band Monte Carlo model," *J. Appl. Phys.*, Vol. 106, No. 6, Art. 063718, 2009.
42. Bertazzi, F., M. Moresco, M. Penna, M. Goano, and E. Bellotti, "Full-band Monte Carlo simulation of HgCdTe APDs," *J. Electron. Mater.*, Vol. 39, No. 7, 912–917, 2010.
43. Bellotti, E., F. Bertazzi, S. Shishehchi, M. Matsubara, and M. Goano, "Theory of carriers transport in III-nitride materials: State of the art and future outlook," *IEEE Trans. Electron Devices*, Vol. 60, No. 10, 3204–3215, 2013.
44. Scharfetter, D. L. and H. K. Gummel, "Large-signal analysis of a silicon read diode transistor," *IEEE Trans. Electron Devices*, Vol. ED-16, No. 1, 64–77, 1969.
45. Ghione, G. and A. Benvenuti, "Discretization schemes for high-frequency semiconductor device models," *IEEE Trans. Antennas Propagation*, Vol. 45, No. 3, 443–456, 1997.
46. Schroeder, D., *Modelling of Interface Carrier Transport for Device Simulation*, Ser. Computational Microelectronics, Springer-Verlag, Wien, 1994.
47. Goano, M., F. Bertazzi, X. Zhou, M. Mandurrino, S. Dominici, M. Vallone, G. Ghione, A. Tibaldi, M. Calciati, P. Debernardi, F. Dolcini, F. Rossi, G. Verzellesi, M. Meneghini, N. Trivellin, C. De Santi, E. Zanoni, and E. Bellotti, "Challenges towards the simulation of GaN-based LEDs beyond the semiclassical framework," *Proc. SPIE*, Vol. 9742, Art. 974202, 2016.
48. De Santi, C., M. Meneghini, A. Tibaldi, M. Vallone, M. Goano, F. Bertazzi, G. Verzellesi, G. Meneghesso, and E. Zanoni, "Physical mechanisms limiting the performance and the reliability of GaN-based LEDs," *Nitride Semiconductor Light-Emitting Diodes*, 2nd Edition, J. J. Huang, H. C. Kuo, and S.-C. Shen, eds., Chap. 14, 455–489, Woodhead Publishing, Duxford, U.K., 2018.
49. Tessler, N. and G. Eisenstein, "On carrier injection and gain dynamics in quantum well lasers," *IEEE J. Quantum Electron.*, Vol. QE-29, No. 6, 1586–1595, 1993.
50. Baraff, G. A., "Semiclassical description of electron transport in semiconductor quantum-well devices," *Phys. Rev. B*, Vol. 55, No. 16, 10 745–10 753, 1997.
51. "Model for the effect of finite phase-coherence length on resonant transmission and capture by quantum wells," *Phys. Rev. B*, Vol. 58, No. 20, 13 799–13 810, 1998.
52. Grupen, M. and K. Hess, "Simulation of carrier transport and nonlinearities in quantum-well laser diodes," *IEEE J. Quantum Electron.*, Vol. 34, No. 1, 120–140, 1998.
53. Alam, M., M. S. Hybertsen, R. Smith, and G. Baraff, "Simulation of semiconductor quantum well lasers," *IEEE Trans. Electron Devices*, Vol. 47, No. 10, 1917–1925, 2000.
54. Hybertsen, M. S., B. Witzigmann, M. A. Alam, and R. K. Smith, "Role of carrier capture in microscopic simulation of multi-quantum-well semiconductor laser diodes," *J. Comp. Electron.*, Vol. 1, No. 1, 113–118, 2002.
55. Gioannini, M., A. P. Cédola, N. Di Santo, F. Bertazzi, and F. Cappelluti, "Simulation of quantum dot solar cells including carrier intersubband dynamics and transport," *IEEE J. Photovoltaics*, Vol. 3, No. 4, 1271–1278, 2013.
56. Engelhardt, A. P., J. S. Kolb, F. Roemer, U. Weichmann, H. Moench, and B. Witzigmann, "Temperature-dependent investigation of carrier transport, injection, and densities in AlGaAs-based multi-quantum-well active layers for vertical-cavity surface-emitting lasers," *Opt. Eng.*, Vol. 54, No. 1, 016 107–1–10, 2015.
57. Vallone, M., F. Bertazzi, M. Goano, and G. Ghione, "Carrier capture in InGaN/GaN quantum wells: Role of electron-electron scattering," *J. Appl. Phys.*, Vol. 121, No. 12, Art. 123107, 2017.
58. Cédola, A. P., D. Kim, A. Tibaldi, M. Tang, A. Khalili, J. Wu, H. Liu, and F. Cappelluti, "Physics-based modeling and experimental study of Si-doped InAs/GaAs quantum dot solar cells," *Indian J. Phys.*, Vol. 2018, 7 215 843–1–10, 2018.
59. Piprek, J., "On the reliability of pulse power saturation models for broad-area GaAs-based lasers," *Opt. Quantum Electron.*, Vol. 51, 60, 2019.
60. Tibaldi, A., F. Bertazzi, M. Goano, M. Daubenschüz, R. Michalzik, and P. Debernardi, "VENUS: A comprehensive electro-thermo-opto VCSEL simulator," *Proc. SPIE*, Vol. 10912, Art. 109120G, 2019.
61. Calciati, M,. A. Tibaldi, F. Bertazzi, M. Goano, and P. Debernardi, "Many-valley electron transport in AlGaAs VCSELs," *Semiconductor Sci. Tech.*, Vol. 32, No. 5, 055007, 2017.

62. Strauss, U., W. W. Rühle, and K. Köhler, "Auger recombination in intrinsic GaAs," *Appl. Phys. Lett.*, Vol. 62, No. 1, 55–57, 1993.
63. Bertazzi, F., M. Goano, and E. Bellotti, "Calculation of Auger lifetime in HgCdTe," *J. Electron. Mater.*, Vol. 40, No. 8, 1663–1667, 2011.
64. Calciati, M., M. Goano, F. Bertazzi, M. Vallone, X. Zhou, G. Ghione, M. Meneghini, G. Meneghesso, E. Zanoni, E. Bellotti, G. Verzellesi, D. Zhu, and C. Humphreys, "Correlating electroluminescence characterization and physics-based models of InGaN/GaN LEDs: Pitfalls and open issues," *AIP Adv.*, Vol. 4, No. 6, Art. 067118, 2014.
65. Bertazzi, F., M. Goano, X. Zhou, M. Calciati, G. Ghione, M. Matsubara, and E. Bellotti, "Looking for Auger signatures in III-nitride light emitters: A full-band Monte Carlo perspective," *Appl. Phys. Lett.*, Vol. 106, No. 6, Art. 061112, 2015.
66. Takeshima, M., "Effect of Auger recombination on laser operation in $Ga_{1-x}Al_xAs$," *J. Appl. Phys.*, Vol. 58, No. 1, 3846–3850, 1985.
67. Mei, S. and I. Knezevic, "Thermal conductivity of III-V semiconductor superlattices," *J. Appl. Phys.*, Vol. 118, 175 101–1–8, 2015.
68. Huo, Y., C. Y. Cho, K. F. Huang, Y. F. Chen, and C. C. Lee, "Exploring the DBR superlattice effect on the thermal performance of a VECSEL with the finite element method," *Opt. Lett.*, Vol. 44, No. 2, 327–330, 2019.
69. Adachi, S., ed., *Properties of Aluminium Gallium Arsenide*, ser. EMIS Datareviews Series, INSPEC, London, 1993.